Keywords:
DWPF
Canister
Thermal Model

Retention: *permanent*

COMSOL Multiphysics Model for DWPF Canister Filling, *Revision 1*

M.R.Kesterson

September 8, 2011

Applied Computational Engineering and Statistics
Savannah River National Laboratory
Aiken, SC 29808

This document was prepared in conjunction with work accomplished under Contract No. DE-AC09-08SR22470 with the U.S. Department of Energy.

SRNL
SAVANNAH RIVER NATIONAL LABORATORY
TM

DISCLAIMER

This document was prepared in conjunction with work accomplished under Contract No. DE-AC09-08SR22470 with the U.S. Department of Energy.

AUTHORS:

M.R, Kesterson, Applied Computational Engineering and Statistics Date
Savannah River National Laboratory

TECHNICAL REVIEWERS:

N.K.Gupta, Applied Computational Engineering and Statistics Date
Savannah River National Laboratory

APPROVERS:

J.W. Amoroso, Customer Date
Process Technology Programs

P.L. Lee, Manager Applied Computational Engineering and Statistics Date
Savannah River National Laboratory

Revision Number:	Page Number:	Date:	Revision:
0	**All**	**3/31/2011**	**Original issue**
1	**All**	**9/8/2011**	**Updated model parameters and resultant simulations based on revised method of incorporating the heat loss in the computer model.**

Table of Contents

List of Tables

List of Figures

1. Introduction and Background

This revision is an extension of the COMSOL Multiphysics model previously developed and documented to simulate the temperatures of the glass during pouring a Defense Waste Processing Facility (DWPF) canister. In that report the COMSOL Multiphysics model used a lumped heat loss term derived from experimental thermocouple data based on a nominal pour rate of 228 lbs./hr. As such, the model developed using the lumped heat loss term had limited application without additional experimental data.

Therefore, the COMSOL Multiphysics model was modified to simulate glass pouring and subsequent heat input which, replaced the heat loss term in the initial model. This new model allowed for changes in flow geometry based on pour rate as well as the ability to increase and decrease flow and stop and restart flow to simulate varying process conditions.

This work was funded by the Department of Energy (DOE) Office of Environmental Management (EM) technology development task EM-31 WP-5.1.2.

2. Model Description

A simplified model for the DWPF canister and interior space consisting of 13,712 elements was created in Comsol Multiphysics and is shown in Figure 1. The geometry of the model was not modified in this revision. The difference between this model and the previous one is the inclusion of a glass stream along the centerline of the container during the pour phase. This section of glass is given a convective heat transfer term based on the velocity of the glass, basically yielding a forced convection term. Radiative heat transfer from the pouring glass stream to the container walls was not used. The model was created with the ability to vary the radius of the glass stream based on the pour rate and height. As a result, there was no fixed glass boundary to use for radiative heat transfer. As before, the model also incorporated heat transfer by conduction and convection in the gas phase.

For initial stabilization of the simulations, the model contained a small region pre-filled with glass with a volume equivalent to the first 10 minutes of pouring. The region is initialized to the thermal properties of the glass with an initial temperature of 100ºC. This region added a buffer to the sudden transition from air to glass and the resultant change in thermal mass within the canister.

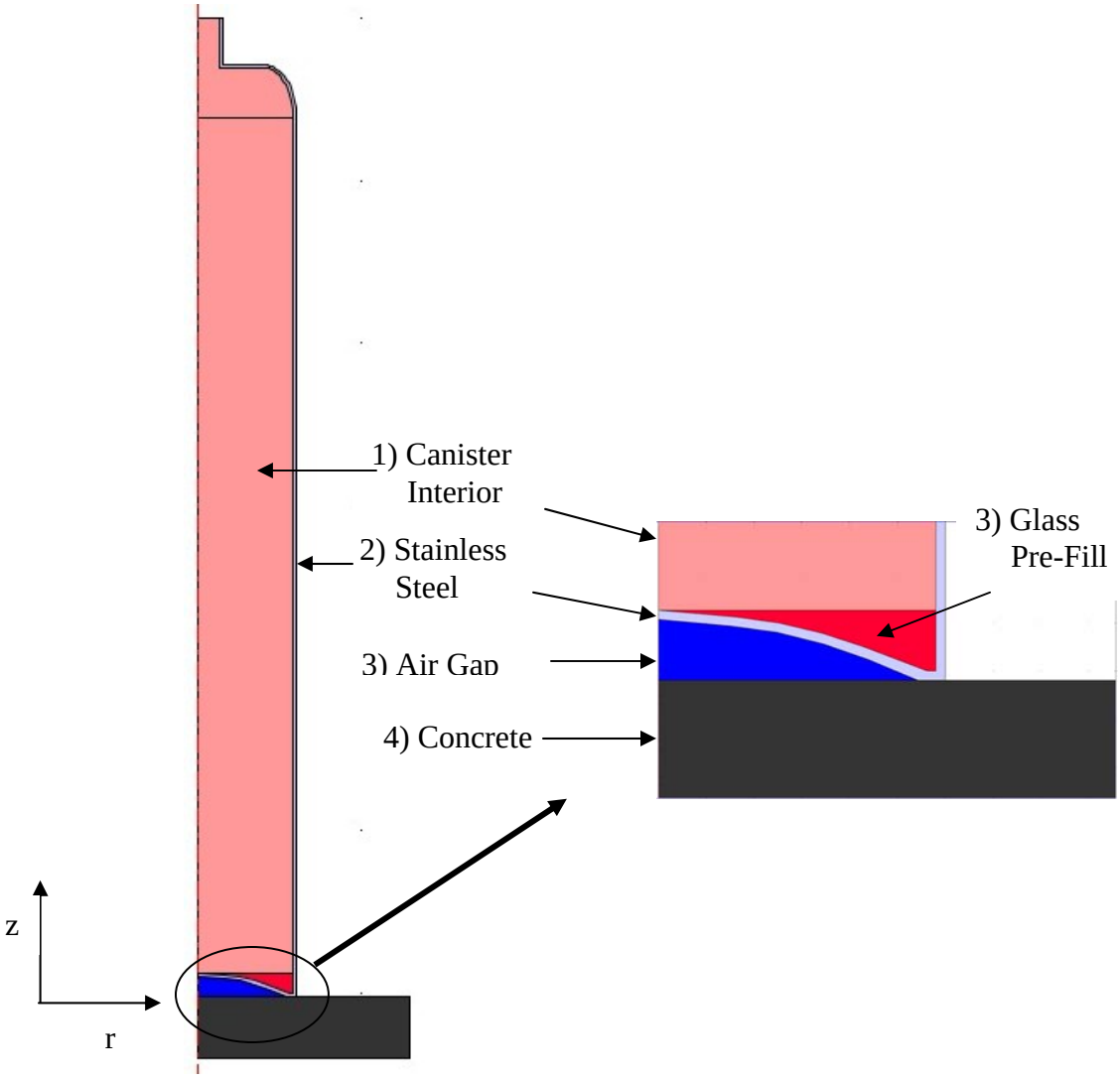

Figure 1 - COMSOL Multiphysics model of the DWPF canister.

The model incorporated convective heat transfer on the outer surface of the canister as the glass via radiative heat transfer from the surface of the glass.

A two-step method was used to model convective heat transfer in the glass phase. The first step was to model the glass stream along the centerline of the container and above the current fluid height. A variable named *glass_r* was used to calculate the radius of the glass stream as a function of pour rate and vertical position within the container. It was assumed that the glass was poured from a spout approximately 1 ft above the entrance of the canister, giving an initial velocity of the glass.

For a system with an initial velocity of 0, the z-displacement is equal to:

$$D = \frac{a}{2} \cdot t^2 \tag{1}$$

Knowing a = 9.8m/s^2, and D = 1 ft, the time to reach the entrance to the canister was calculated. Next, the velocity of the glass when it reaches the canister opening was calculated by:

$$v = a \cdot t \tag{2}$$

With the calculated velocity, and knowing the volumetric flowrate of the glass, the cross-sectional area of the glass can be obtained, and therefore the entrance *glass_r* value.

$$A = \frac{V}{v} \tag{3}$$

$$t = \sqrt{\frac{2 \cdot (3.3048 - z)}{a}} \tag{4}$$

$$v = \sqrt{2 \cdot a \cdot (3.3048 - z)} \tag{5}$$

$$glass\_r_{entrance} = \sqrt{\frac{A}{\pi}} \tag{6}$$

Where z = height(m), and the 3.3048 term is the combination of the canister height plus 1 foot above for the assumed pour height.

Applying a velocity increase due to gravity, the radius of the glass column was obtained as a function of the vertical height.

$$glass\_r = \sqrt{\frac{V}{\pi \cdot \sqrt{2 \cdot a \cdot (3.3048 - z)}}} \tag{7}$$

where V = volumetric flowrate (m^3/s); a = acceleration (m/s^2), and z = height(m).

Once the falling glass reached the current fill height, the convective heat transfer term was changed from a vertical flow to a radial flow. The maximum z velocity (calculated at the bottom of the canister) was used as the base value, multiplied by a power function, decreasing the velocity of the glass as it flows radially outward. The general form of the equation is:

$$v_{glass\_radial} = C \cdot \left(\frac{R_{inner\_Wall} - r}{R_{inner\_Wall}} \right)^{(5+5\cdot(z<0.25))} \quad (8)$$

where

v_{glass_radial} = velocity of the glass flowing in the radial direction (m/s)
R_{inner_Wall} = Inside radius of the canister (m)
C = Base radial velocity 0.08 (m/s)
r = radius at which the equation is evaluated (m)
z = Height at which the equation is evaluated (m)

The value for C along with the exponential factor were determined through simulation trial and error fits to the radial and vertical temperature profile seen in the experimental data.

3. Inputs and Assumptions

Below are the inputs and assumptions that are used in the COMSOL model. All units reported below are used in the model. The COMSOL model has a base unit system of SI, but the user is allowed to input properties in any units and COMSOL converts them to the base unit system for calculations.

Assumptions:

3.1. The ambient temperature in the room is a constant 26ºC. The experimental data shows that the room temperature had variations between 24ºC and 30ºC [0] with an average room temperature that was approximately 26ºC.

3.2. Radiation and convective heat transfer in the enclosed air space between the canister bottom and the ground is accounted for by an increased thermal conductivity term.

3.3. The experimental data used was based on scale glass melter run with a nominal pour rate of 228 lb/hr [0]. In reviewing the experimental data, the actual flow rate varied between 190 and 360 lb/hr. A step function was employed in the model to approximate the flow rate variation and more accurately match the experimental conditions. The function is shown in Appendix A – Global Expressions table

Inputs:

3.4. Glass pour temperature is 1080ºC

3.5. Canister dimensions are supplied on drawing W747391 [0]

3.6. Material Properties – Table 1 and Table 2

Table 1 - Material Properties of Canister

Material	Thermal Conductivity		Density (lb_m/ft^3)	Specific Heat	
Stainless Steel Canister [0]	$\frac{BTU}{hr \cdot ft \cdot {}^oF}$	Temperature (ºF)	494.429	$\frac{BTU}{lb_m \cdot {}^oF}$	Temperature (ºF)
	3.9915	-328			
	6.28963	-148		0.120	32
	7.74108	32			
	9.43444	212		0.135	752
	12.5793	932			
	14.9983	1292		0.135	3000
	14.9983	3000			

Table 2 - Material Properties of DWPF glass

Material	Thermal Conductivity		Density		Specific Heat	
Glass [0]	$\frac{BTU}{hr \cdot ft \cdot {}^oF}$	Temperature (ºF)	(lb_m/ft^3)	Temperature (ºF)	$\frac{BTU}{lb_m \cdot {}^oF}$	Temperature (ºF)
					0.204	20
	0.76449	20	172.31	20	0.204	68
					0.24	212
	0.76449	68	171.37	392	0.272	392
					0.295	572
	0.76449	1742	167.31	932	0.312	752
					0.325	932
	1.3741	1832	165.44	112	0.334	1112
					0.342	1292
	2.8063	2012	162.94	1292	0.349	1472
					0.354	1652
	3.5079	2102	160.45	1472	0.356	1740
					0.358	1832
	3.5079	3000	157.95	1652	0.362	2012
					0.363	2102
			151.77	2192	0.365	2192
					0.365	3000

The model consisted of two additional regions requiring material properties. These regions were the floor below the canister and the air initially contained within the canister and the air trapped between the canister and the concrete floor. The floor was modeled as

a concrete slab with a lower temperature boundary condition equal to the ambient air temperature. The material library contained within COMSOL is used to obtain the material properties for both the air and concrete.

4. Methodology

Based on the time of the simulation and the time step, a corresponding volume of glass was added to the system by changing the material properties of the subdomain in the region between the calculated new glass height and the previous glass height (glass_height(t) – glass_height(dt)). The material properties for this region were changed from air to those of the glass, specifically changing the specific heat, density, and thermal conductivity. At the same time, the radial heat flow term, (Eq 8), adds heat to the new glass region.

Multiple simulations were run in order to obtain the constants in the radial glass velocity equations. The constants were obtained by using an initial guess, running the simulation and comparing the simulated results to the experimental data. Based on the outcome of the comparison, the constants were modified and the simulations re-run. This process was repeated multiple times until the simulation results approximated the experimental data.

5. Results

5.1. Glass Pouring Model

Figures Figure 2 toFigure 6 show the final results obtained from the model at five thermocouple locations: 1) bottom surface of the canister, 2) 15 inches, 3) 51 inches, 4) 87 inches, and 5) 99 inches. The larger temperature differences predicted at the 99 inch height are due to the lack of internal radiation from the top surface of the glass to the interior canister walls.

As seen in the following figures, the temperatures of the glass and the canister surface predicted using the model compare relatively well with the experimental data for both filling and cooling. For the end time of 3000 minutes, the simulations predict a temperature of approximately 30ºC higher, at the 87 inch thermocouple, than the experimental data.

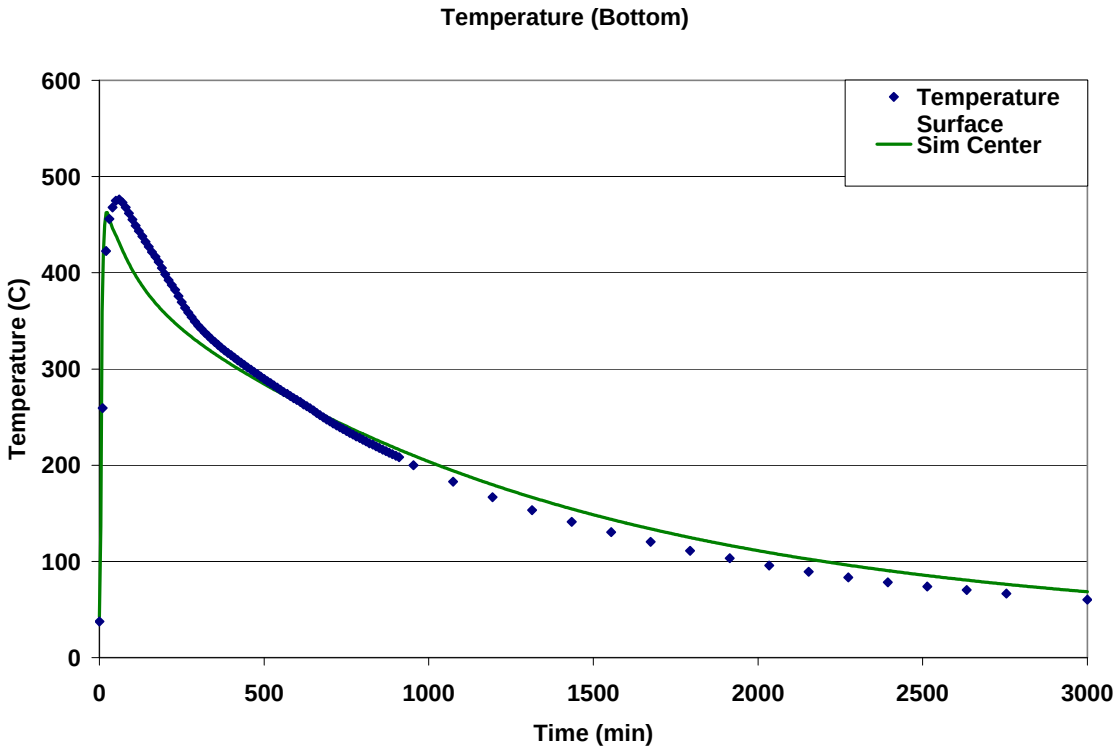

Figure 2 - Temperature curves for thermocouple and simulation data located on the outside bottom of the canister.

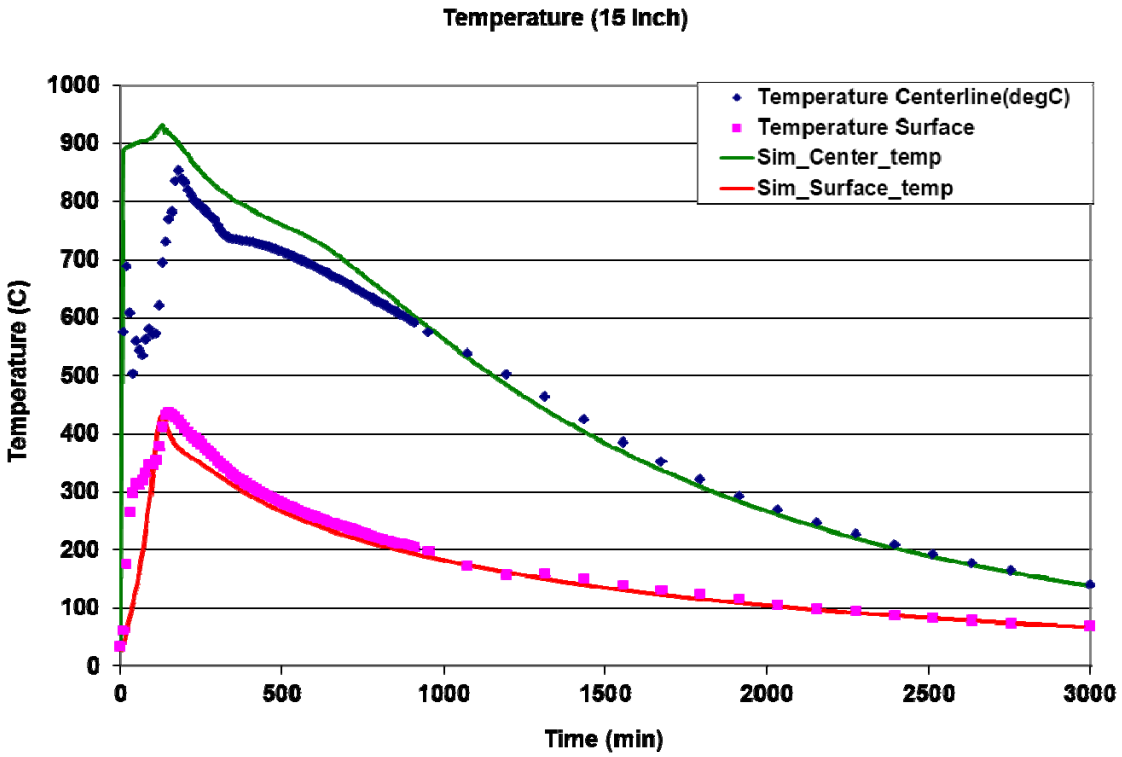

Figure 3 - Temperature curves for thermocouple and simulation data at the 15 inch location of the canister.

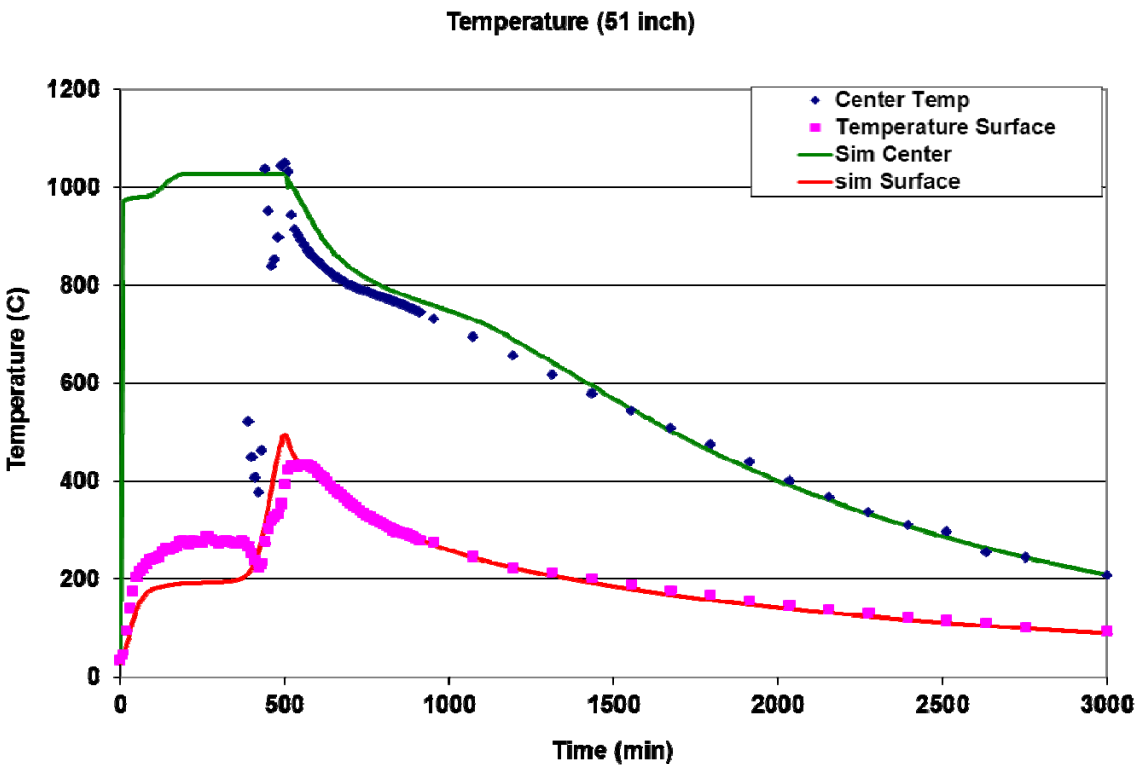

Figure 4 - Temperature curves for thermocouple and simulation data at the 51 inch location of the canister.

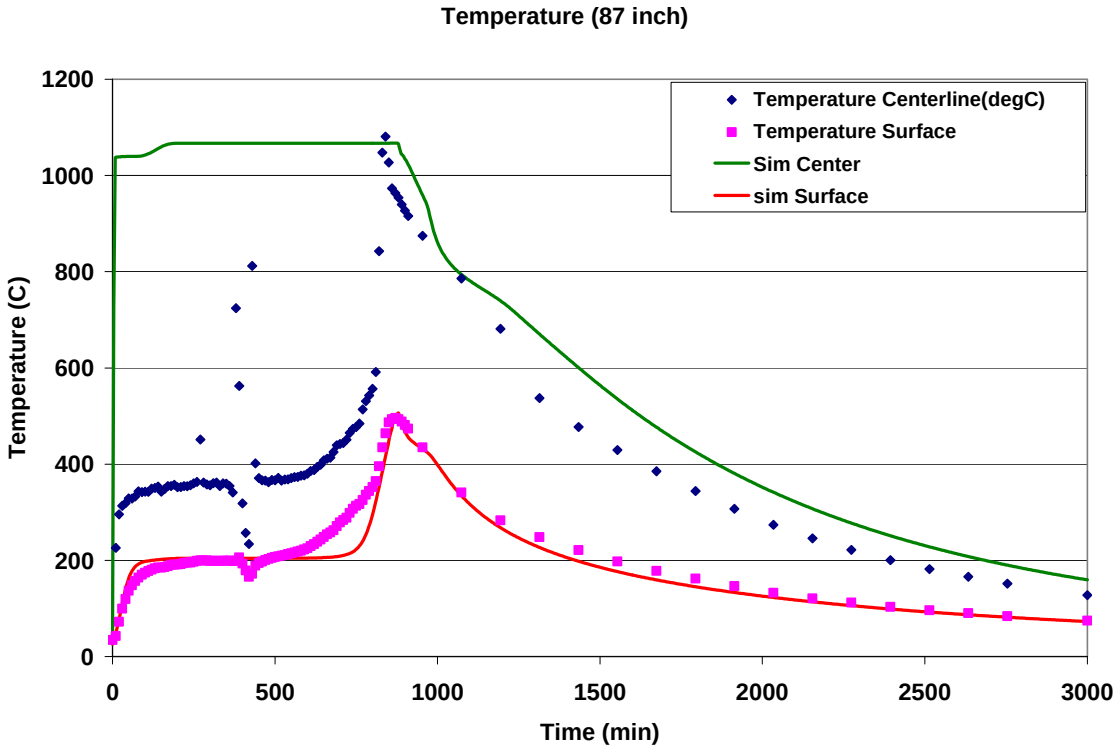

Figure 5 - Temperature curves for thermocouple and simulation data at the 87 inch location of the canister.

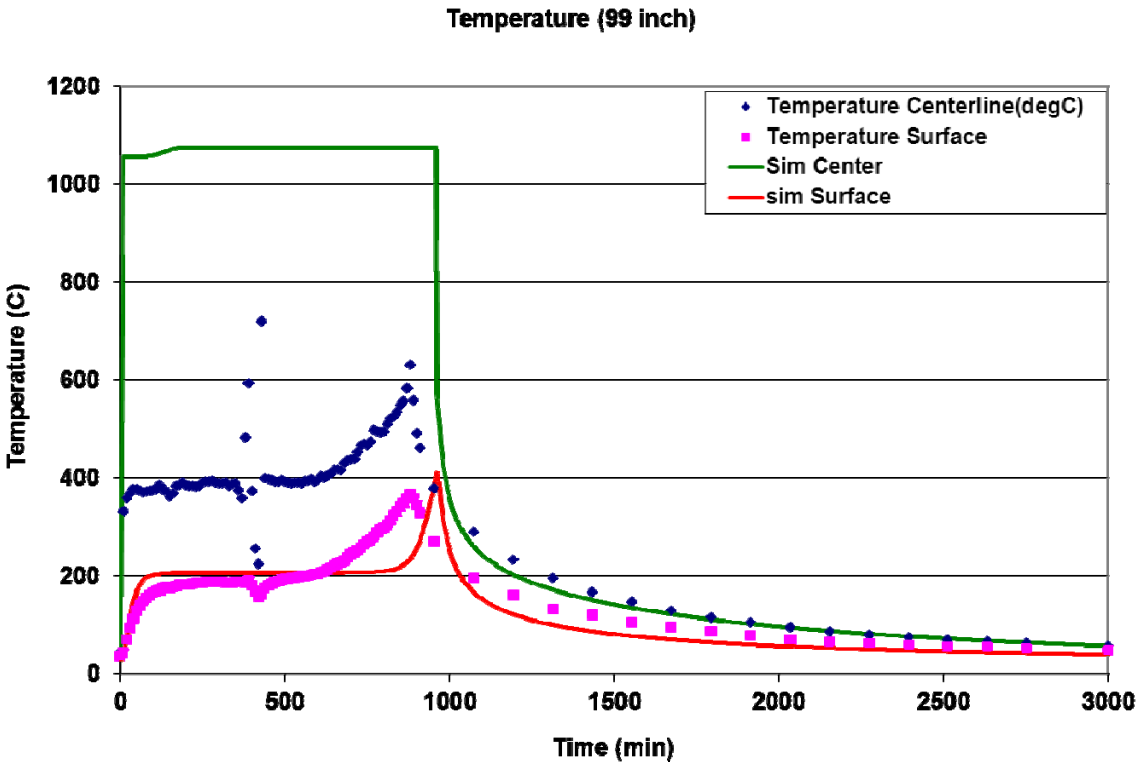

Figure 6 - Temperature curves for thermocouple and simulation data at the 99 inch location of the canister.

As seen in the thermocouple plots, there is a large difference in the simulated temperature and the experimental temperature for all of the centerline thermocouples prior to the fill level reaching the thermocouple height. This is due to the simulation pouring glass down the exact centerline of the canister thereby covering the simulation thermocouple location with hot glass.

6. Conclusions

A revised COMSOL Multiphysics model was developed to predict temperatures of the glass within DWPF canisters during filling and cooldown. The model simulations and experimental data were in good agreement. The largest temperature deviations were ~ 40°C for the 87inch thermocouple location at 3000 minutes and during the initial cool down at the 51 inch location occurring at approximately 600 minutes. Additionally, the model described in this report predicts the general temperature trends during filling and cooling as observed experimentally.

The revised model incorporates a heat flow region corresponding to the glass pouring down the centerline of the canister. The geometry of this region is dependent on the flow rate of the glass and can therefore be used to see temperature variations for various pour rates. The equations used for this model were developed by comparing simulation output to experimental data from a single pour rate. Use of the model will predict temperature profiles for other pour rates but the accuracy of the simulations is unknown due to only a single flow rate comparison.

7. References

1. COMSOL Multiphysics, Version 3.5a, COMSOL Inc, Burlington, MA.

2. J.R. Fowler, R.E. Edwards, S.L. Marra, and M.J. Plodinec, "*Chemical Composition Projections for then DWPF Product*", WSRC-IM-91-116-1, Rev. 1, 1995.

3. Drawing - W747391, "*Savannah River Plant Bldg 221S 200 Area DWPF – CDC Canister Assembly Mechanical*", 1984.

4. D.A. Tamburello, "*Predicting Temperatures for AFCI Canistered Waste Glasses*", Interoffice Memorandum, SRNL-L5200-2009-00013, 2009.

8. Appendix

Appendix A - Comsol Constants and Expressions

The following tables are the constants and global expressions directly exported from COMSOL.

COMSOL Constants

Constant Name	Constant Value	Description
gravity	9.8[m/s^2]	Acceleration due to gravity
glass_rho	167[lb/ft^3]	Glass Density as a constant
inlet_area	0.031416[m^2]	Opening at the top of the canister
Lower_area	0.26512[m^2]	Cross-sectional area of the canister
glass_T_init	1080[degC]	Inlet glass temperature
sigma	5.67e-8[W/m^2/K^4]	
T_atm	26[degC]	Ambient Temperature
SS_rho	494.429[lb/ft^3]	Density of stainless steel
ContainerHeight	3[m]	Height of the canister
dt	40[s]	Simulation timestep
MaxGlass	3656[lb]	Amount of glass added to the canister
MaxHeight	MaxGlass/glass_rho/Lower_area	Maximum height of the glass
T_Lump_init	100[degC]	Initial temperature of the lower glass region
int_emmisivity	0.55[1]	Internal emissivity
P_atm	1[atm]	Internal air pressure
PourRate	228	Unitless pour rate
PourRateUnit	PourRate*1[lb/h]	Pour rate with units
AirMaxFlow	.1[m/s]	Maximum internal air velocity
BaseFlow	228[lb/h]	Flow rate of the experimental data

COMSOL Global Expressions

Vaiable Name	Expression	Description
Fluid_Height	(Fluid_Height_new+0.07)*Filling+MaxHeight*(1-Filling)	Current Glass Height
T_amb	25[degC]	Ambient Temperature
delHeight	(z<=Fluid_Height)*(z>LastFluidHeight)[1]	Switch for z between the current and last fluid height
Ra_init	gravity*Beta*(T-T_atm)*ContainerHeight^3/(air_visc*air_k/air_rho^2/air_cp)	
Ra	Ra_init*(Ra_init>0)	
Beta	1/T	
Pr	air_cp*air_visc/air_k	
h_surface_low	(air_k/ContainerHeight)*(0.68+(0.670*Ra^.25)/(1.0+(0.492/Pr)^(9/16))^(4/9))	

Vaiable Name	Expression	Description
h_surface_high	((air_k/ContainerHeight)*(0.825+(0.387*Ra^(1/6))/(1.0+(0.492/Pr)^(9/16))^(8/27))^2)	
h_surface	(h_surface_low*(Ra<=1e9)+h_surface_high*(Ra>1e9))	Heat transfer coefficient for the outside surface of the canister
T_min	T*(T>T_atm-5)+T_atm*(T<=T_atm-5)	
Filling	((Fluid_Height_new+.01[m])<=MaxHeight)[1]	Switch for flow on/off
Q_rad_top	sigma*((glass_T_init)^4-(T)^4)*Filling	
emmisivity	.85[1]	External emissivity of the canister
glassFlow1	128[lb/h]*t*(t<=905[min])	Flowrate of glass for the first time period.
glassFlow2	(228[lb/h]*(t-905[min])+glw1)*(t>905[min])	Flowrate of glass for the second time period.
glassFlow3	(228[lb/h]*(t-270[min])+glw1+glw2)*(t>270[min])*(t<=350[min])	Flowrate of glass for the third time period.
glassFlow4	(228[lb/h]*(t-350[min])+glw1+glw2+glw3)*(t>350[min])*(t<=500[min])	Flowrate of glass for the fourth time period.
glassFlow5	(228[lb/h]*(t-500[min])+glw1+glw2+glw3+glw4)*(t>500[min])*(t<=610[min])	Flowrate of glass for the fifth time period.
glassFlow6	(228[lb/h]*(t-610[min])+glw1+glw2+glw3+glw4+glw5)*(t>610[min])*(t<=730[min])	Flowrate of glass for the sixth time period.
glassFlow7	(228[lb/h]*(t-730[min])+glw1+glw2+glw3+glw4+glw5+glw6)*(t>730[min])	Flowrate of glass for the seventh time period.
glw1	128[lb/h]*905[min]	Mass of glass accumulated during the first time period
glw2	228[lb/h]*90[min]	Mass of glass accumulated during the second time period
glw3	228[lb/h]*80[min]	Mass of glass accumulated during the third time period
glw4	228[lb/h]*150[min]	Mass of glass accumulated during the fourth time period
glw5	228[lb/h]*110[min]	Mass of glass accumulated during the fifth time period
glw6	228[lb/h]*120[min]	Mass of glass accumulated during the sixth time period
Fluid_Height_new_const	PourRateUnit*t/glass_rho/Lower_area	Fluid height calculated with a constant pour rate
Fluid_Height_new	(glassFlow1+glassFlow2)/glass_rho/Lower_area	Fluid height calculated using step changes in flow rate
glassFlow1_dt	128[lb/h]*(t-dt)*(t<=905[min])	Mass of glass accumulated during the first time period-the timestep
glassFlow2_dt	(228[lb/h]*(t-dt-905[min])+glw1)*(t>905[min])	Mass of glass accumulated during the second time period-the timestep
glassFlow3_dt	(228[lb/h]*(t-dt-270[min])+glw1+glw2)*(t>270[min])*(t<=350[min])	Mass of glass accumulated during the third time period-the timestep

Vaiable Name	Expression	Description
glassFlow4_dt	(228[lb/h]*(t-dt-350[min])+glw1+glw2+glw3)*(t>350[min])*(t<=500[min])	Mass of glass accumulated during the fourth time period-the timestep
glassFlow5_dt	(228[lb/h]*(t-dt-500[min])+glw1+glw2+glw3+glw4)*(t>500[min])*(t<=610[min])	Mass of glass accumulated during the fifth time period-the timestep
glassFlow6_dt	(228[lb/h]*(t-dt-610[min])+glw1+glw2+glw3+glw4+glw5)*(t>610[min])*(t<=730[min])	Mass of glass accumulated during the sixth time period-the timestep
glassFlow7_dt	(228[lb/h]*(t-dt-730[min])+glw1+glw2+glw3+glw4+glw5+glw6)*(t>730[min])	Mass of glass accumulated during the seventh time period-the timestep
LastFluidHeight_const	PourRateUnit*(t-dt)/glass_rho/Lower_area+0.07[m]	Fluid height from previous timestep if constant pour rate is used.
LastFluidHeight	((glassFlow1_dt+glassFlow2_dt)/glass_rho/Lower_area)+0.06[m]	Fluid height from previous timestep if variable pour rate is used.
z_vel_air	-0.7*(flc2hs(z[1/m]-(Fluid_Height[1/m]+0.2),0.2))*(0.15-r[1/m])*z_vel_glass_base*(r>glass_r)*TimeFact*Filling	
r_vel_air	-0.7*(z>Fluid_Height)*r_vel_air_base*(1-flc2hs(z[1/m]-2.74,0.1))*(r>glass_r)*TimeFact*Filling	
r_vel_air_base	AirMaxFlow*(-44.444*(r[1/m])^2+13.333333*r[1/m])	
Entrance_Temp	((glass_T_init-T_atm)*TimeFact+T_atm)*Filling+T*(1-Filling)	Inlet glass temperature with ramping factor
z_vel_glass	z_vel_glass_base*flc2hs(glass_r[1/m]-r[1/m],0.0001)*flc2hs(z[1/m]-(Fluid_Height[1/m]+delHeight),delHeight)*Filling	Velocity of falling glass based on height
glass_r	sqrt(PourRateUnit/glass_rho/pi/sqrt(2*gravity*(3.3048-z)*Filling	Radius of the glass centerline
TimeFact	flc2hs(t[1/s]-400,400)[1]	Ramping factor for start of simulation
r_glass_vel	(-0.1*((0.295-r[1/m])/0.295)^(5+5*flc2hs(0.25-Fluid_Height[1/m],0.1))+.00008)*delHeight*(r>glass_r)*Filling*FlowFactor	Radial glass velocity at the current glass height
z_vel_glass_base	-(9.8*((3.3048-z[1/m])/4.9)^(0.5))[m/s]	Velocity of centerline glass based on gravity
FlowFactor	(128[lb/h]+100[lb/h]*flc2hs(t[1/min]-905,10))/BaseFlow	
SS_cp	(.12+.015*flc2hs(T[1/degF]-452[degF][1/degF],300))[Btu/lb/degF]	Heat capacity of stainless steel
SS_k	(-13.589083+3.9578316*log(T_min[1/K]))[Btu/h/ft/degF]	Thermal conductivity of stainless steel
glass_k	(1+0.2*flc2hs(T[1/degC]-400,200)+8.5*flc2hs(T[1/degC]-800,100))[Btu/h/ft/degF]*0.9	Temperature dependent thermal conductivity for the glass phase
glass_rho_adap	(172.31*(T[degC]<20)+(T[degC]>=20)*(T[degC]<=1200)*(172.2011+.00109*T[1/degC]-1.609e-5*(T[1/degC])^2-1.508162e-8*(T[1/degC])^3+1.3323e-11*(T[1/degC])^4)+151.77*(T[degC]>1200))[lb/ft^3]	Temperature dependent density for the glass phase
glass_cp	(0.45+0.2*flc2hs(T[1/degC]-600,400))[Btu/lb/degF]	Temperature dependent heat capacity for the glass phase

Vaiable Name	Expression	Description
k_eff	((200*air_k+100*air_k*(r[1/m]<glass_r[1/m]+0.03))*(z>Fluid_Height)+(2*glass_k-300*air_k)*(r[1/m]<=glass_r[1/m])*(z[1/m]>Fluid_Height[1/m]))*Filling+glass_k*(z[1/m]<=Fluid_Height[1/m])+10*air_k*(z>Fluid_Height)*(1-Filling)	Thermal conductivity of the region inside the canister. k changes from air to glass based on fluid height.
Cp_eff	air_cp*(z>Fluid_Height)+glass_cp*(z<=Fluid_Height)+(glass_cp-air_cp)*(r[1/m]<=glass_r[1/m])	Heat capacity of the region inside the canister. Cp changes from air to glass based on fluid height.
rho_eff	air_rho*(z>Fluid_Height)+glass_rho_adap*(z<=Fluid_Height)+(glass_rho_adap-air_rho)*(r[1/m]<=glass_r[1/m])*(z>Fluid_Height)	Density of the region inside the canister. Density changes from air to glass based on fluid height.
air_k	mat3_k(T[1/K])[W/(m*K)]	Air thermal conductivity
air_rho	mat3_rho(P_atm[1/Pa],T[1/K])[kg/m^3]	Air density
air_cp	mat3_Cp(T[1/K])[J/(kg*K)]	Air heat capacity

Appendix B - Simulation Temperature versus Time Data

Time (min)	Bottom Surface (C)	15 Inch Center (C)	15 Inch Surface (C)	51 Inch Center (C)	51 Inch Surface (C)	87 Inch Center (C)	87 Inch Surface (C)	99 Inch Center (C)	99 Inch Surface (C)
0	42.67	26.00	26.05	26.00	26.00	26.00	26.00	26.00	26.00
20	462.34	892.71	62.61	976.63	70.39	1038.67	78.40	1057.26	80.28
40	446.14	898.20	112.12	979.25	119.18	1039.27	140.66	1057.40	151.06
60	431.19	901.92	168.45	980.70	154.07	1039.53	178.08	1057.45	185.48
80	416.14	904.84	240.89	981.67	172.39	1039.86	192.54	1057.63	197.71
100	402.88	912.15	340.44	986.27	180.03	1042.46	197.63	1059.39	201.95
120	391.54	926.19	427.00	996.23	183.60	1048.26	199.83	1063.35	203.70
140	381.58	923.82	414.92	1009.01	186.19	1055.73	201.33	1068.46	204.80
160	372.71	912.01	388.76	1020.31	188.50	1062.33	202.60	1072.97	205.70
180	364.71	899.52	375.29	1026.64	190.28	1066.03	203.53	1075.50	206.38
200	357.44	884.83	366.71	1027.89	191.27	1066.75	204.01	1076.00	206.74
220	350.73	870.12	359.38	1027.90	191.68	1066.76	204.17	1076.00	206.87
240	344.51	856.43	352.04	1027.90	191.94	1066.76	204.22	1076.00	206.91
260	338.68	844.24	344.48	1027.91	192.22	1066.76	204.24	1076.00	206.93
280	333.18	833.44	336.82	1027.91	192.61	1066.76	204.24	1076.00	206.93
300	327.96	823.81	329.19	1027.92	193.18	1066.76	204.24	1076.00	206.93
320	322.98	815.14	321.70	1027.93	194.11	1066.76	204.25	1076.00	206.94
340	318.19	807.27	314.44	1027.95	195.64	1066.76	204.25	1076.00	206.94
360	313.57	800.05	307.43	1027.97	198.64	1066.76	204.25	1076.00	206.94
380	309.10	793.37	300.70	1028.00	205.36	1066.76	204.25	1076.00	206.94
400	304.75	787.13	294.25	1028.05	222.02	1066.76	204.25	1076.00	206.94
420	300.51	781.25	288.09	1028.12	257.63	1066.76	204.26	1076.00	206.94
440	296.38	775.66	282.19	1028.23	316.54	1066.76	204.26	1076.00	206.94
460	292.32	770.29	276.55	1028.38	386.69	1066.76	204.27	1076.00	206.94
480	288.35	765.08	271.17	1028.59	457.38	1066.76	204.28	1076.00	206.94
500	284.45	759.95	266.01	1028.85	495.00	1066.76	204.30	1076.00	206.94
520	280.62	754.85	261.07	1001.27	460.42	1066.76	204.33	1076.00	206.94
540	276.85	749.69	256.33	981.82	440.53	1066.76	204.38	1076.00	206.95
560	273.14	744.40	251.79	957.15	430.24	1066.76	204.45	1076.00	206.95
580	269.49	738.87	247.42	932.30	420.46	1066.76	204.55	1076.00	206.96
600	265.89	732.98	243.22	909.53	409.89	1066.76	204.72	1076.00	206.98
620	262.34	726.59	239.17	889.80	398.84	1066.76	204.98	1076.00	207.00
640	258.84	719.59	235.27	873.09	387.74	1066.76	205.39	1076.00	207.03
660	255.40	711.95	231.51	858.93	376.94	1066.76	206.02	1076.00	207.09
680	252.00	703.80	227.87	846.73	366.57	1066.76	207.06	1076.00	207.17
700	248.65	695.31	224.35	836.06	356.68	1066.77	208.80	1076.00	207.29
720	245.34	686.60	220.95	826.61	347.31	1066.77	211.95	1076.00	207.49
740	242.09	677.77	217.65	818.16	338.45	1066.78	217.91	1076.00	207.81
760	238.87	668.90	214.45	810.52	330.09	1066.80	230.13	1076.00	208.30
780	235.71	660.08	211.34	803.55	322.20	1066.82	253.88	1076.00	209.07
800	232.59	651.39	208.32	797.13	314.76	1066.85	295.01	1076.00	210.37
820	229.51	642.67	205.38	791.18	307.73	1066.90	351.78	1076.00	212.53
840	226.48	633.82	202.53	785.61	301.09	1066.98	415.66	1076.01	216.21
860	223.49	624.89	199.74	780.36	294.80	1067.07	475.02	1076.02	222.84
880	220.55	615.93	197.03	775.37	288.84	1065.94	506.51	1076.03	235.50

900	217.65	606.96	194.39	770.58	283.18	1033.97	466.79	1076.04	258.94
920	214.79	598.00	191.80	765.95	277.80	1008.89	448.63	1076.07	296.74
940	211.98	589.07	189.28	761.44	272.68	979.33	438.46	1076.11	348.07
960	209.21	580.19	186.82	756.98	267.79	950.76	428.71	569.31	410.70
980	206.48	571.40	184.41	752.55	263.12	905.76	416.45	425.98	313.13
1000	203.79	562.69	182.05	748.09	258.65	861.14	398.75	355.51	250.41
1020	201.14	554.08	179.74	743.54	254.38	834.38	379.52	316.40	215.07
1040	198.53	545.57	177.49	738.85	250.27	816.13	361.35	289.79	191.81
1060	195.96	537.18	175.27	733.92	246.32	802.21	344.81	270.14	175.06
1080	193.43	528.91	173.10	728.68	242.53	790.77	329.91	254.75	162.25
1100	190.94	520.77	170.98	723.03	238.87	780.85	316.48	242.14	152.01
1120	188.49	512.75	168.89	716.89	235.35	771.81	304.33	231.49	143.55
1140	186.07	504.86	166.84	710.22	231.94	763.24	293.29	222.28	136.38
1160	183.70	497.11	164.84	703.06	228.65	754.74	283.21	214.17	130.20
1180	181.36	489.48	162.86	695.54	225.47	745.96	273.95	206.94	124.78
1200	179.05	481.98	160.93	687.79	222.38	736.49	265.42	200.40	119.97
1220	176.79	474.61	159.03	679.86	219.39	726.01	257.51	194.44	115.67
1240	174.55	467.37	157.16	671.84	216.48	714.57	250.17	188.97	111.78
1260	172.36	460.25	155.32	663.81	213.66	702.58	243.31	183.90	108.24
1280	170.19	453.26	153.51	655.92	210.92	690.53	236.90	179.18	105.00
1300	168.06	446.39	151.74	648.42	208.24	678.57	230.88	174.77	102.02
1320	165.97	439.65	149.99	640.65	205.64	666.69	225.21	170.63	99.26
1340	163.90	433.01	148.28	632.74	203.10	654.94	219.87	166.72	96.70
1360	161.87	426.50	146.59	624.73	200.62	643.29	214.81	163.03	94.31
1380	159.87	420.10	144.93	616.67	198.20	631.67	210.01	159.53	92.08
1400	157.90	413.80	143.30	608.58	195.83	620.11	205.45	156.19	89.99
1420	155.97	407.62	141.69	600.48	193.52	608.64	201.12	153.02	88.01
1440	154.06	401.54	140.11	592.40	191.26	597.26	196.98	149.98	86.16
1460	152.18	395.57	138.55	584.34	189.04	586.00	193.03	147.08	84.40
1480	150.33	389.69	137.02	576.34	186.86	574.89	189.25	144.29	82.73
1500	148.52	383.92	135.51	568.38	184.73	563.94	185.63	141.62	81.16
1520	146.73	378.24	134.02	560.50	182.64	553.16	182.16	139.05	79.65
1540	144.96	372.66	132.56	552.69	180.59	542.57	178.82	136.57	78.22
1560	143.23	367.17	131.12	544.97	178.58	532.17	175.61	134.19	76.86
1580	141.52	361.77	129.71	537.33	176.60	521.97	172.52	131.88	75.56
1600	139.84	356.46	128.31	529.80	174.65	511.97	169.54	129.66	74.31
1620	138.18	351.24	126.94	522.36	172.74	502.17	166.67	127.51	73.12
1640	136.56	346.11	125.58	515.03	170.86	492.58	163.89	125.43	71.98
1660	134.95	341.06	124.25	507.80	169.01	483.20	161.21	123.41	70.88
1680	133.37	336.09	122.94	500.67	167.19	474.01	158.61	121.46	69.83
1700	131.82	331.20	121.65	493.66	165.40	465.04	156.09	119.56	68.81
1720	130.29	326.39	120.37	486.75	163.63	456.25	153.65	117.72	67.84
1740	128.78	321.66	119.12	479.95	161.90	447.67	151.28	115.94	66.90
1760	127.30	317.01	117.89	473.26	160.19	439.28	148.98	114.20	65.99
1780	125.84	312.43	116.67	466.68	158.50	431.07	146.74	112.51	65.12
1800	124.40	307.93	115.47	460.20	156.84	423.05	144.57	110.87	64.27
1820	122.99	303.51	114.29	453.82	155.20	415.21	142.45	109.28	63.46
1840	121.60	299.15	113.13	447.55	153.59	407.55	140.40	107.72	62.67
1860	120.23	294.87	111.98	441.37	152.00	400.05	138.39	106.21	61.91
1880	118.88	290.65	110.85	435.30	150.43	392.73	136.44	104.73	61.17
1900	117.55	286.51	109.74	429.33	148.89	385.57	134.54	103.29	60.45

1920	116.24	282.43	108.64	423.45	147.36	378.57	132.68	101.89	59.76
1940	114.95	278.42	107.56	417.66	145.86	371.73	130.87	100.52	59.09
1960	113.68	274.48	106.50	411.97	144.38	365.03	129.10	99.19	58.43
1980	112.43	270.60	105.45	406.36	142.92	358.49	127.37	97.89	57.80
2000	111.20	266.78	104.41	400.85	141.48	352.09	125.68	96.61	57.19
2020	109.99	263.03	103.40	395.42	140.06	345.84	124.03	95.37	56.59
2040	108.80	259.35	102.39	390.08	138.66	339.72	122.42	94.16	56.01
2060	107.62	255.72	101.40	384.82	137.27	333.74	120.84	92.97	55.44
2080	106.47	252.15	100.43	379.64	135.91	327.89	119.30	91.81	54.89
2100	105.33	248.65	99.46	374.54	134.57	322.17	117.79	90.68	54.36
2120	104.21	245.20	98.52	369.52	133.24	316.57	116.32	89.57	53.84
2140	103.10	241.81	97.58	364.58	131.93	311.10	114.87	88.49	53.33
2160	102.02	238.48	96.66	359.71	130.64	305.75	113.45	87.43	52.84
2180	100.95	235.20	95.76	354.92	129.37	300.51	112.07	86.39	52.35
2200	99.89	231.98	94.86	350.19	128.12	295.39	110.71	85.37	51.89
2220	98.85	228.81	93.98	345.54	126.88	290.38	109.38	84.38	51.43
2240	97.83	225.70	93.11	340.96	125.66	285.48	108.08	83.41	50.98
2260	96.82	222.64	92.25	336.45	124.45	280.69	106.80	82.46	50.55
2280	95.83	219.63	91.41	332.01	123.26	276.00	105.55	81.52	50.12
2300	94.86	216.67	90.57	327.63	122.09	271.41	104.32	80.61	49.71
2320	93.89	213.76	89.75	323.32	120.93	266.93	103.12	79.71	49.30
2340	92.95	210.90	88.94	319.07	119.79	262.54	101.94	78.84	48.91
2360	92.01	208.09	88.14	314.88	118.66	258.24	100.78	77.98	48.52
2380	91.10	205.33	87.35	310.76	117.55	254.04	99.64	77.13	48.14
2400	90.19	202.62	86.58	306.69	116.45	249.93	98.53	76.31	47.77
2420	89.30	199.95	85.81	302.69	115.37	245.91	97.43	75.50	47.41
2440	88.42	197.32	85.06	298.75	114.30	241.97	96.36	74.71	47.06
2460	87.56	194.74	84.31	294.86	113.25	238.12	95.31	73.93	46.72
2480	86.70	192.20	83.58	291.04	112.21	234.35	94.27	73.16	46.38
2500	85.87	189.71	82.85	287.26	111.19	230.66	93.26	72.42	46.05
2520	85.04	187.26	82.14	283.55	110.17	227.05	92.26	71.68	45.73
2540	84.22	184.85	81.43	279.89	109.17	223.52	91.28	70.96	45.41
2560	83.42	182.48	80.74	276.29	108.19	220.06	90.32	70.25	45.10
2580	82.63	180.15	80.05	272.73	107.21	216.67	89.38	69.56	44.80
2600	81.85	177.85	79.38	269.24	106.25	213.36	88.45	68.88	44.50
2620	81.09	175.60	78.71	265.79	105.30	210.11	87.54	68.21	44.21
2640	80.33	173.38	78.05	262.40	104.37	206.93	86.64	67.56	43.93
2660	79.59	171.20	77.41	259.05	103.45	203.82	85.76	66.91	43.65
2680	78.86	169.06	76.77	255.76	102.53	200.77	84.90	66.28	43.37
2700	78.13	166.95	76.14	252.52	101.63	197.78	84.05	65.66	43.11
2720	77.42	164.88	75.51	249.32	100.75	194.85	83.22	65.05	42.84
2740	76.72	162.84	74.90	246.17	99.87	191.99	82.40	64.46	42.59
2760	76.03	160.83	74.29	243.08	99.00	189.18	81.59	63.87	42.34
2780	75.35	158.86	73.70	240.02	98.15	186.43	80.80	63.29	42.09
2800	74.68	156.92	73.11	237.02	97.30	183.73	80.02	62.73	41.85
2820	74.02	155.01	72.53	234.06	96.47	181.09	79.25	62.17	41.61
2840	73.37	153.14	71.95	231.14	95.65	178.50	78.50	61.62	41.37
2860	72.73	151.29	71.39	228.27	94.84	175.96	77.76	61.09	41.15
2880	72.10	149.47	70.83	225.44	94.03	173.47	77.03	60.56	40.92
2900	71.48	147.69	70.28	222.66	93.24	171.03	76.31	60.04	40.70
2920	70.86	145.93	69.73	219.92	92.46	168.63	75.61	59.53	40.49

2940	70.26	144.20	69.20	217.22	91.69	166.29	74.92	59.03	40.27
2960	69.66	142.50	68.67	214.56	90.93	163.99	74.23	58.54	40.07
2980	69.08	140.82	68.15	211.94	90.17	161.73	73.56	58.06	39.86
3000	68.50	139.18	67.63	209.36	89.43	159.52	72.90	57.58	39.66

Distribution

J. W. Amoroso, 999-W
A. B. Barnes, 999-W
C. L. Crawford, 773-42A
D. A. Crowley, 773-43A
A. P. Fellinger, 773-41A
S. D. Fink, 773-A
K. M. Fox, 999-W
B. J. Giddings, 786-5A
N.K. Gupta, 703-41A
C. C. Herman, 999-W
C. M. Jantzen, 773-A
F. C. Johnson, 999-W
M.R. Kesterson, 703-41A
P.L. Lee, 703-41A
S. L. Marra, 773-A
D. K. Peeler, 999-W
F. M. Pennebaker, 773-42A
M. E. Stone, 999-W
D.A. Tamburello, 703-41A
W. R. Wilmarth, 773-A